EFFICIENT LARGE-EDDY SIMULATIONS OF LOW MACH NUMBER FLOWS USING PRECONDITIONING AND MULTIGRID

BAMDAD LESSANI[1] JAN RAMBOER [1] CHRIS LACOR [1]

[1] *Department of Fluid Mechanics, Vrije Universiteit Brussel, Pleinlaan 2, 1050 Brussel, Belgium*

Abstract

In the present paper an implicit time accurate approach combined with multigrid and preconditioning is used for the large-eddy simulation of low Mach number flows. It will be shown that the present approach allows an efficiency gain of a factor 4 to 7 compared to the use of a purely explicit approach. The efficiency varies according to the test case, grid clustering, physical time step and requested residual drop.

1 Introduction

Preconditioning is widely used as a convergence accelerationtool for low Mach number flows. This technique, however, is not time accurate excluding its straightforward use for unsteady problems. Multigrid on the other hand is one of the most efficient convergence acceleration tools. In practice, most multigrid applications are for steady state problems. The dual time-stepping approach can be used for time accurate problems and has the advantage that non-time accurate tools such as preconditioning, multigrid, residual smoothing and local time stepping can be used in a time accurate context. In the present paper the use of these methods is extended towards large-eddy simulations of low Mach number flows.

The LES code is an extension of the finite volume Reynolds Averaged Navier-Stokes (RANS) solver EURANUS, [1]. EURANUS contains an efficient multigrid solver based on the Full Approximation Storage (FAS) scheme for flows ranging from low subsonic up to hypersonic, [2][3]. The Runge-Kutta scheme acts as a smoother for the multigrid. For low Mach number flows, the efficiency of multigrid strongly depends on the stiffness of the equation and the ability of the smoother to damp the high frequency errors. The stiffness is removed with the preconditioning technique which was applied successfully to different steady and unsteady RANS flows, [4][2], and in the present paper will be used in the LES context. A central second-order finite volume spatial discretization is used in the LES code. Fourth-order artificial dissipation is added to increase the high frequency damping of the smoother. In order to avoid laminarization of the flow, the artificial dissipation is only added to the continuity equation but not to the momentum and energy equations. According to our experience, this also suffices to guarantee a good overall convergence. As mentioned above, dual time-stepping is used to update the equations in time. The physical time derivative is discretized either by a backward differencing method or by a trapezoidal scheme. Numerical experiments show that the trapezoidal scheme is more flexible and allows bigger time steps as compared to the backward differencing.

The Smagorinsky model is used for subgrid-scale modeling. Both the classical model and the dynamic model, [7], are available in the code.

2 Mathematical Formulation

The preconditioning procedure in the framework of dual time-stepping can be formulated as, [2]:

$$\frac{1}{\beta^2}\frac{\partial \overline{p}}{\partial \tau}+\frac{\partial \overline{\rho}}{\partial t}+\frac{\partial \overline{\rho}\tilde{u}_i}{\partial x_i}=0 \tag{1}$$

$$\frac{(1+\alpha)\tilde{u}_i}{\beta^2}\frac{\partial \overline{p}}{\partial \tau}+\overline{\rho}\frac{\partial \tilde{u}_i}{\partial \tau}+\frac{\partial \overline{\rho}\tilde{u}_i}{\partial t}+\frac{\partial \overline{\rho}\tilde{u}_i\tilde{u}_j}{\partial x_j}=-\frac{\partial \overline{p}}{\partial x_i}+\frac{\partial \widetilde{\sigma_{ij}}}{\partial x_j}-\frac{\partial \tau_{ij}}{\partial x_j} \tag{2}$$

$$(\frac{\alpha\tilde{u}_i^2+\tilde{H}-\beta^2}{\beta^2})\frac{\partial \overline{p}}{\partial \tau}+\overline{\rho}\frac{\partial \tilde{H}}{\partial \tau}+\frac{\partial \overline{\rho}\tilde{E}}{\partial t}+\frac{\partial(\overline{\rho}\tilde{E}\tilde{u}_j+\overline{p}\tilde{u}_j)}{\partial x_j}=\frac{\partial \widetilde{\sigma_{ij}}\tilde{u}_i}{\partial x_j}-\frac{\partial \tilde{q}_j}{\partial x_j}-\frac{\partial Q_j}{\partial x_j} \tag{3}$$

Where τ is the pseudo-time, t the physical time and $\widetilde{\sigma_{ij}}$, τ_{ij} respectively the filtered stresses and SGS stresses:

$$\widetilde{\sigma_{ij}}=\tilde{\mu}(\frac{\partial \tilde{u}_i}{\partial x_j}+\frac{\partial \tilde{u}_j}{\partial x_i}-\frac{2}{3}\frac{\partial \tilde{u}_k}{\partial x_k}\delta_{ij}) \tag{4}$$

$$\tau_{ij}=\bar{\rho}(\widetilde{u_iu_j}-\tilde{u}_i\tilde{u}_j)=-\mu_t(\frac{\partial \tilde{u}_i}{\partial x_j}+\frac{\partial \tilde{u}_j}{\partial x_i}-\frac{2}{3}\frac{\partial \tilde{u}_k}{\partial x_k}\delta_{ij}) \tag{5}$$

The subgrid-scale heat-flux Q_i is defined as:

$$Q_i=\bar{\rho}c_p(\widetilde{T\tilde{u}_i}-\tilde{T}\tilde{u}_i) \tag{6}$$

It is modeled using an eddy diffusivity SGS model:

$$Q_i=-\frac{\mu_t c_p}{Pr_t}\frac{\partial \tilde{T}}{\partial x_i} \tag{7}$$

$\mu_t=\rho C\Delta^2|\tilde{S}|$, and $Pr_t=0.5$ or is calculated dynamically. β and α are the preconditioning parameters. α is taken as a constant around -1, and β can be defined locally as, [9],

$$\beta=Min(Max(\sqrt{u_iu_i},\frac{\nu}{\Delta},\frac{l}{\pi\Delta t}),c) \tag{8}$$

With Δ the smallest cell length, l the biggest characteristic dimension of the domain, Δt the physical time step and c the speed of sound. In the present LES calculations Δt is rather small, due to physical restrictions, such that $\frac{l}{\pi\Delta t}$ is the dominant term in (8). As a result, β will be constant on the whole field.

By applying the finite volume method to (1), (2) and (3), they can be written in matrix form as follows:

$$\Gamma^{-1}\frac{\partial Q\Omega}{\partial \tau}+\frac{\partial U\Omega}{\partial t}=Res \tag{9}$$

Written out fully:

$$\begin{bmatrix} \frac{1}{\beta^2} & 0 & 0 & 0 & 0 \\ \frac{(1+\alpha)\tilde{u}_1}{\beta^2} & \overline{\rho} & 0 & 0 & 0 \\ \frac{(1+\alpha)\tilde{u}_2}{\beta^2} & 0 & \overline{\rho} & 0 & 0 \\ \frac{(1+\alpha)\tilde{u}_3}{\beta^2} & 0 & 0 & \overline{\rho} & 0 \\ \frac{\alpha\tilde{u}_i^2+\tilde{H}-\beta^2}{\beta^2} & 0 & 0 & 0 & \overline{\rho} \end{bmatrix} \begin{bmatrix} \overline{p}_{,\tau}\Omega \\ \tilde{u}_{1,\tau}\Omega \\ \tilde{u}_{2,\tau}\Omega \\ \tilde{u}_{3,\tau}\Omega \\ \tilde{H}_{,\tau}\Omega \end{bmatrix} + \begin{bmatrix} \overline{\rho}_{,t}\Omega \\ (\overline{\rho}\tilde{u}_1)_{,t}\Omega \\ (\overline{\rho}\tilde{u}_2)_{,t}\Omega \\ (\overline{\rho}\tilde{u}_3)_{,t}\Omega \\ (\overline{\rho}\tilde{E})_{,t}\Omega \end{bmatrix} = - \begin{bmatrix} \int \overline{\rho}\tilde{u}_jn_jdS \\ \int(\overline{\rho}\tilde{u}_j\tilde{u}_1+\overline{p}\delta_{1j}+\tau_{1j}-\widetilde{\sigma_{1j}})n_jdS \\ \int(\overline{\rho}\tilde{u}_j\tilde{u}_2+\overline{p}\delta_{2j}+\tau_{2j}-\widetilde{\sigma_{2j}})n_jdS \\ \int(\overline{\rho}\tilde{u}_j\tilde{u}_3+\overline{p}\delta_{3j}+\tau_{3j}-\widetilde{\sigma_{3j}})n_jdS \\ \int((\overline{\rho}\tilde{E}+\overline{p})\tilde{u}_j+\tilde{q}_j+Q_j-\widetilde{\sigma_{ij}}\tilde{u}_i)njdS \end{bmatrix} \tag{10}$$

The physical time derivative ($\frac{\partial U\Omega}{\partial t}$) is discretized with a multi-step scheme:

$$\Gamma^{-1}\frac{\partial Q\Omega}{\partial \tau} = -\frac{\beta_1}{\Delta t}U\Omega + S^n + \gamma_1 Res(U) \tag{11}$$

where S^n is the source term defined as:

$$S^n = -\frac{\beta_0}{\Delta t}(U^n\Omega) - \frac{\beta_{-1}}{\Delta t}(U^{n-1}\Omega) - \frac{\beta_{-2}}{\Delta t}(U^{n-2}\Omega) + \gamma_2 Res(U^n) \tag{12}$$

by multiplying both sides of (11) by Γ

$$\frac{\partial Q\Omega}{\partial \tau} = \Gamma(-\frac{\beta_1}{\Delta t}U\Omega + S^n + \gamma_1 Res(U)) \tag{13}$$

Now a Runge-Kutta method can be used to reach the steady state in pseudo-time. For stability reasons the $\frac{\beta_1}{\Delta t}U$ term is treated implicitly within the Runge-Kuta cycle, for example the i stage is written as,

$$Q^i + \alpha_i \Delta\tau \Gamma \frac{\beta_1 U^i}{\Delta t} = Q^0 + \alpha_i \frac{\Delta\tau}{\Omega}\Gamma(S^n + \gamma_1 Res(U^{i-1})) \qquad i = 1, q \tag{14}$$

after some algebraic manipulations,

$$Q^i = Q^0 + (I + \Gamma\alpha_i\Delta\tau\frac{\beta_1}{\Delta t}\frac{\partial U}{\partial Q})^{-1}\alpha_i\frac{\Delta\tau}{\Omega}\Gamma(-\frac{\beta_1 U^{i-1}\Omega}{\Delta t} + S^n + \gamma_1 Res(U^{i-1})) \tag{15}$$

Calculation of $(I+\Gamma\alpha_i\Delta\tau\frac{\beta_1}{\Delta t}\frac{\partial U}{\partial Q})^{-1}$ in a general compressible case is computationally very expensive. For the sake of simplicity, incompressibility is assumed for the evaluation of $\frac{\partial U}{\partial Q}$. The matrix equals,

$$(I + \Gamma\alpha_i\Delta\tau\frac{\beta_1}{\Delta t}\frac{\partial U}{\partial Q})^{-1} = \begin{bmatrix} 1 & 0 & 0 & 0 & 0 \\ 0 & \frac{1}{1+\alpha_i\frac{\beta_1\Delta\tau}{\Delta t}} & 0 & 0 & 0 \\ 0 & 0 & \frac{1}{1+\alpha_i\frac{\beta_1\Delta\tau}{\Delta t}} & 0 & 0 \\ 0 & 0 & 0 & \frac{1}{1+\alpha_i\frac{\beta_1\Delta\tau}{\Delta t}} & 0 \\ 0 & 0 & 0 & 0 & \frac{1}{1+\alpha_i\frac{\beta_1\Delta\tau}{\Delta t}} \end{bmatrix} \tag{16}$$

This simplification seems to be accurate enough and has not brought any convergence problem for the test cases considered so far.

3 Results

The efficiency of the dual time-stepping method depends on the number of inner iterations (n_1) and the ratio of the physical time step to the time step of a purely explicit scheme ($n_2 = \frac{\Delta t}{\Delta\tau}$). The gain achieved will be n_2/n_1. As a result, the main goal is to choose the physical time step (Δt) as large as possible and make the number of inner iterations (n_1) as small as possible.

This section is divided into three parts, the first part is about the method of discretizing the physical time derivative and its effect on the maximum allowable time step (Δt), in the second part the beneficial effect of preconditioning and multigrid on the requested number of inner iterations is demonstrated and finally some LES results of the channel, cavity and circular cylinder flows are presented.

3.1 Relation Between the Time Integration and the Physical Time Step

It is a well known fact that the backward differencing scheme unlike the trapezoidal scheme has a dissipation error proportional to the time step. In order to see this effect and its influence on the LES results a channel flow at $Re_\tau = 180$ with a mesh of $33 \times 33 \times 65$ points in the x, y and z directions is considered. The time derivative is discretized either with a backward differencing ($\beta_1 = 1.5$, $\beta_0 = -2$, $\beta_{-1} = 0.5$, $\beta_{-2} = 0.0$, $\gamma_1 = 1.$ and $\gamma_2 = 0.0$) or a trapezoidal scheme ($\beta_1 = 1.$, $\beta_0 = 0.0$, $\beta_{-1} = -1$, $\beta_{-2} = 0.0$, $\gamma_1 = 0.5$ and $\gamma_2 = 0.5$) Figures (1) and (2) show the mean velocity profile and the turbulence intensities calculated with the backward differencing scheme and the trapezoidal scheme, respectively.

The trapezoidal scheme is much more flexible than the backward differencing for large time steps. By increasing the time step, the results start deviating from the reference solution (obtained with an explicit time accurate Runge-Kutta method) at $\Delta t = 0.005$ for the backward differencing and at $\Delta t = 0.02$ for the trapezoidal scheme. This behavior is in accordance with the flat plate boundary layer results of Weber *et al.*[11]. The results are also compared with the DNS data of Kim *et al.*[12], the discrepancy between the LES and DNS results is due to the use of a second-order scheme used for the spatial discretization on a relatively coarse mesh. By using higher order methods more accurate results can be obtained, [10].

3.2 The Effect of Preconditioning on Multigrid

The success of multigrid depends on the ability of the smoother to remove the high frequency errors which cannot be supported on coarser meshes. For low Mach number flows preconditioning is necessary to remove the stiffness of the equations and to increase the high frequency damping ability of the smoother.

A test was carried out on the channel flow at $Re_\tau = 180$, M=0.06 with a mesh of $33 \times 33 \times 33$ points. Figure (3) shows part of the convergence graph for four combinations of multigrid and preconditioning. The number of inner iterations is fixed to 50.

When preconditioning is not used there is almost no difference between single grid and multigrid, but when preconditioning is activated multigrid becomes quite efficient.

When both preconditioning and multigrid are switched off, the residual drop of the first momentum equation is around one order of magnitude, and for the continuity equation is less than two. When both preconditioning and multigrid are used, the residual drops are more than four and three orders of magnitude for the first momentum and continuity equations, respectively. Due to the addition of artificial dissipation, the multigrid works more efficiently for the continuity equation than for the first momentum equation in which the artificial dissipation is switched off. For these calculations $\alpha = -1$ and β is globally defined as $\beta^2 = 3.V_{cent}^2$, where V_{cent} is the velocity at the centerline of the channel. A three-level V-sawtooth multigrid is used.

3.3 Some LES Results

In all calculations a second-order central discretization is used in space and a second-order trapezoidal scheme in time. A five-stage Runge-Kutta scheme, $\alpha = \{\frac{1}{4}, \frac{1}{6}, \frac{3}{8}, \frac{1}{2}, 1\}$, $\beta = \{1, 0, 0.56, 0, 0.44\}$ with three evaluations of dissipation, [6], is used as the smoother for the multigrid. A three-level V-sawtooth multigrid with a first order prolongation and quadratic restriction is used.

3.3.1 Channel Flow

The rotating and non-rotating channel flows are considered. For the non-rotating channel flow, a mesh of $33 \times 33 \times 65$ points is used in the x, y and z directions, the streamwise, normal and spanwise dimensions are $4\pi \times 2 \times 2\pi$. Uniform meshes with spacing $\Delta x^+ = \frac{\Delta x u_\tau}{\nu} \simeq 71$ and $\Delta z^+ = \frac{\Delta z u_\tau}{\nu} \simeq 18$ are used in the streamwise and spanwise directions. A non uniform mesh with cosinus distribution is

used in the wall-normal direction. The first mesh point away from the wall is at $y^+ = \frac{\Delta y u_\tau}{\nu} \simeq 0.87$ and the maximum spacing (at the centerline of the channel) is 18 wall units. The Reynolds number based on the friction velocity is $Re_\tau = 180$ and the Mach number at the centerline is $M = 0.06$. A dynamic procedure, [7], is used to calculate the Smagorinsky coefficient and the turbulent Prandtl number. For this calculation $\alpha = -1$ and $\beta^2 = 3.U^2_{center}$.

For the rotating channel flow, the same mesh is used and the results of the non-rotating channel were used as the initial solution. The rotation number is equal to $Ro = 0.01$. The rotation number based on the bulk mean velocity (U_m), angular velocity (Ω) and channel half width (h) is,

$$Ro = \frac{2\Omega h}{U_m} \tag{17}$$

The turbulence intensities are shown in Fig. (4), the results are compared with the DNS data of Kim *et al.*[12] and Kristoffersen *et al.* [13].

The physical time step is around 200 times bigger than the time step of a purely explicit method, the residual drop of the continuity equation is fixed to -2.5 and this requires almost 50 inner iterations. The gain achieved is roughly equal to $\frac{200}{50} = 4$.

3.3.2 Cavity Flow

A lid driven cavity flow is considered as another example to test the ability of the present approach. The flow is driven by the top wall, $z = h$, in the x direction moving with a velocity $U = 1$. The Reynolds number is $Re = \frac{Uh}{\nu} = 10000$ where h is the dimension of the cube. A 33^3 mesh is used with a cosinus distribution of the mesh points. Starting from a stagnant flow, the flow is fully developed after $32h/U$, after which statistics were collected during a period of $32h/U$. The mean velocity profiles along the vertical and horizontal symmetry lines and the statistics of the fluctuating field are shown in Fig. 5. The agreement between the experiment, [14], and simulation is satisfactory. A Smagorinsky model with damping near the wall is used for subgrid scale modeling. For this calculation $\alpha = -1$ and $\beta^2 = 10.U^2$. The physical time step (Δt) is around 1000 times bigger than the maximum time step allowed by the stability condition of an explicit scheme in a compressible flow. In almost 130 inner iterations the residual of the continuity equation drops four orders of magnitude. As a rough estimation, and without taking into account the extra work of the multigrid, the implicit approach is around $1000/130 \simeq 7.5$ times faster than a purely explicit approach.

3.3.3 Circular Cylinder

The cylinder has a diameter of D and a spanwise length of πD at a Reynolds number of $Re_D = 3900$. In the plane normal to the cylinder axis, an O-type grid with 49×81 points is used with 81 points on the surface and 49 points in the radial direction, 33 grid points is used over the spanwise length of πD. The mesh is clustered near the wall to ensure $y^+ < 1$ for the first grid point. A Smagorinsky model with damping near the wall is used for subgrid-scale modeling. For this calculation $\alpha = -1$ and $\beta^2 = 3.U^2_\infty$. The flow statistics are compared with the experimental data of Lourenco and Shih, taken from, [16]. Statistics were accumulated over $T = 60D/U_\infty$. The distribution of the pressure coefficient c_p and the friction coefficient c_f on the cylinder are plotted in Fig. 6. In the same figure the mean streamwise velocity component along the centerline is shown.

Figure 7 shows the velocity fluctuations at $X = \frac{x - x_l}{x_l} = -0.0806$, with x_l the location where the time averaged streamwise velocity component is zero.

The residual drop of the continuity equation is fixed to -2. which is obtained after 100 inner iterations. The physical time step of the implicit method is around 400 times bigger than the time step of the explicit one. The implicit method is $\frac{400}{100} = 4$ times faster than the explicit method.

4 Conclusions

Preconditioning and multigrid have been used for large-eddy simulation of low Mach number flows. A dual time-stepping approach was used to keep the time accuracy of the simulation. The channel and cavity flows as well as the flow around a circular cylinder have been considered to test the ability of the method. It was shown that the present method was 4 to 7 times faster than a purely explicit approach. The efficiency varies according to the test case, grid clustering, physical time step and requested residual drop.

5 Aknowledgments

This research work was partially funded by the Flemish Science Foundation (FWO) under the grant G.0170.98. This support is gratefully acknowledged.

References

[1] Lacor C., Zhu Z. W. and Hirsch Ch.,"*A New Family of Limiters within the Multigrid/Multiblock Navier-Stokes Code EURANUS*", AIAA/DGLR 5th International Aerospace Planes and Hypersonics Technologies Conference, AIAA 93-5023, 1993.

[2] Hirsch Ch. and Hakimi N., "*Preconditioning Methods for Time-Marching Navier-Stokes Solvers*", Solution Techniques for Large-Scale CFD Problems, CMAS, John Wiley and Sons, pp. 333-353, 1995.

[3] Zhu Z. W., Alavilli P., Lacor C., and Hirsch Ch., "*Efficiency and Robustness of Multigrid Methods for Hypersonic Flows*", AIAA 97-0342, 1997.

[4] Hirsch Ch. and Hakimi N., "*Preconditioning Methods for Time-Marching Navier-Stokes Solvers*", International Workshop on Solution Techniques for Large-Scale CFD Problems, 26-28 Sep, CERCA, Montral, Quebec, Canada, 1994.

[5] Darmofal D. L. and Van Leer B., "*Local Preconditioning of the Euler Equations: A Characteristic Interpretation*", Von Karman Lecture Series 1999-03, March 8-12, 1999.

[6] Jameson A., "*Time Dependent Calculations Using Multigrid, With Applications to Unsteady Flows past Airfoils and Wings*", AIAA 91-1596, 1991.

[7] Germano M., Piomelli U., Moin P. and Cabot W. H., "*A Dynamic Subgrid-Scale Eddy Viscosity Model*", Physics of Fluids A, **3**, 1991.

[8] Piomelli U. and Liu J.,"*Large-Eddy Simulation of Rotating Channel Flows Using a Localized Dynamic Model*, Physics of Fluids, **7**, 1995.

[9] Venkateswaran S. and Merkle L., "*Analysis of Preconditioning Methods for the Euler and Navier-Stokes Equations*", Von Karman Lecture Series, 1999-03, March 8-12,1999.

[10] Smirnov S., Lacor Ch. and Baelmans M., "*A Finite Volume Formulation for Compact Scheme with Applications to LES*", AIAA 2001-2546.

[11] Weber C., Ducros F., and Corjon A., "*Assessment of Implicit Time Accurate Integration for LES*", AIAA 99-3355, pp. 866-876.

[12] Kim J., Moin P. and Moser R., "*Turbulence Statistics in Fully Developed Channel Flow at Low Reynolds Number*", Journal of Fluid Mechanics, 177, 133-166.

[13] Kristoffersen R., Andersson H. I., "*Direct Numerical Simulations of Low-Reynolds Number Turbulent Flow in a Rotating Channel*", Journal of Fluid Mechanics, 256, 163-197.

[14] Prasad A. K. and Koseff J. R., "*Reynolds Number and End-Wall Effects on a Lid Driven Cavity Flow*", Physics of Fluids, **1**, 1989.

[15] Leriche E. and Gavrilakis S., "*Direct Numerical Simulation of the Flow in a Lid-Driven Cubical Cavity*", Physics of Fluids, **12**, 2000.

[16] Kravchenko A. G. and Moin P., "*Numerical Studies of Flow Over a Circular Cylinder at* $Re_D =$ 3900", Physics of Fluids, **12**, 2000.

[17] Breuer M., "*Large Eddy Simulation of the Subcritical Flow Past a Circular Cylinder: Numerical and Modeling Aspect*", International Journal for Numerical Methods in Fluids, **28**, 1998.

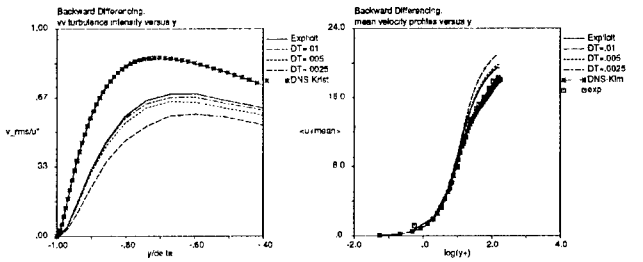

Figure 1: Effect of the time step with the backward-differencing

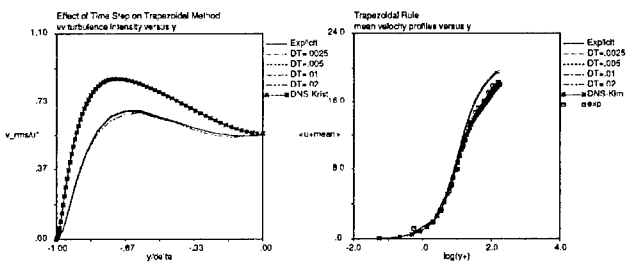

Figure 2: Effect of the time step with the trapezoidal scheme

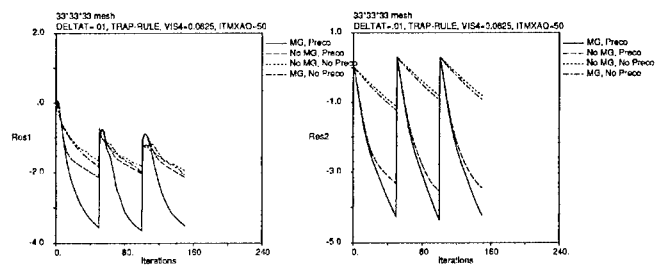

Figure 3: The effect of preconditioning on multigrid for the channel flow calculation with a fixed number of inner iterations, left: continuity equation, right: first momentum equation

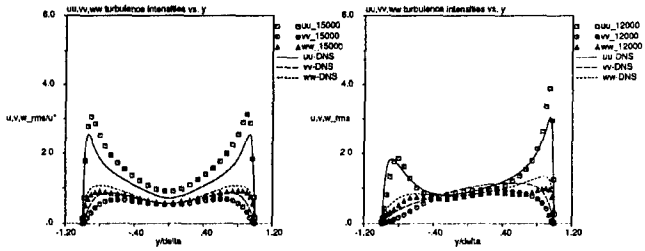

Figure 4: Turbulence intensities, left: non rotating channel flow, right: rotating channel flow

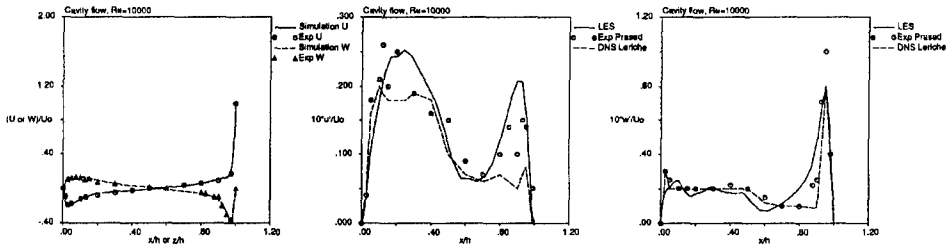

Figure 5: (left): mean velocity profile along two symmetry lines, (middle): $10\sqrt{u'u'}/U$, (right): $10\sqrt{w'w'}/U$, lines are used for the simulation data and markers for experimental data.

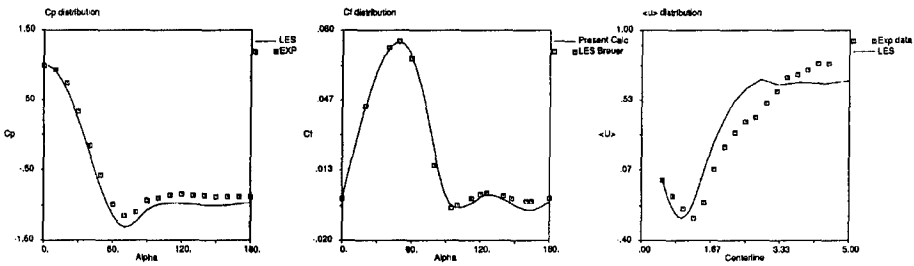

Figure 6: (left): c_p distribution, (middle): c_f distribution, $\circ$ LES of Breuer [17] (right): mean streamwise velocity, c_p and $< u >$ are compared with the experiment of Lourenco and Shih [16]

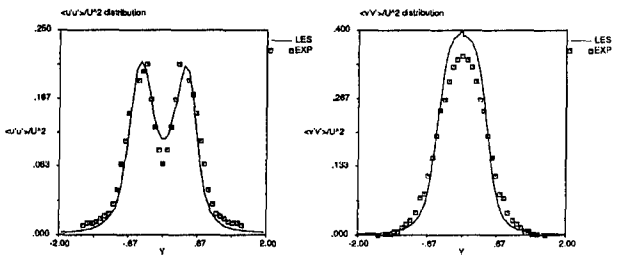

Figure 7: (left): velocity fluctuations at $X = \frac{x-x_l}{x_l} = -0.0806$, $\diamond$, experiment of Lourenco and Shih [16]